Available online at https://ifejost.oauife.edu.ng

IFE JOURNAL OF SCIENCE AND TECHNOLOGY

Vol 8. No. 1 (2024) 93 – 101

Enhanced photabsorption and supercapacitive potentials of MnS thin film electrode with Li-ions incorporation for optoelectronic and energy storage applications

Adeyeye, M. O.[1], Akinade, A. G.[1], Olatinwo, A. S.[1], Adewinbi, S. A.[2], Adewumi, O. E.[1], Animasahun, L. O.[3], Omotoso, E.[1] and Taleatu, B. A.[1,*]

[1]Department of Physics and Engineering Physics, Obafemi Awolowo University, Ile-Ife, Nigeria
[2]Department of Physics, Osun State University, Osogbo, Osun State, Nigeria
[3]Department of Physics, Electronics and Earth Sciences, Fountain University, Osogbo, Nigeria
[*]Corresponding Author's Email: bdntaleatuoauife.edu.ng

Abstract

MnS and lithium-doped MnS thin films were prepared on Indium Tin Oxide (ITO) conductive substrates from appropriate inorganic chemical reagents using two-electrode electrochemical deposition technique. Effects of Li-ions incorporation as dopant impurity on some surface properties of the thin film: optical, electrical and electrochemical cyclic voltammetry responses, were investigated to explore the films' optoelectronic and energy storage potentials. The optical result showed high absorbance in the UV region and high transmittance towards visible and infrared spectra wavelength range of EM spectrum. Direct allowed transition with decreasing energy band gap value from 2.03 eV to 1.85 eV relative to lithium dopant concentration was observed. The film also revealed increasing surface conductivity with thickness. Enhanced electrochemical charge storage of the MnS host material leading to specific capacitance value of 95 F g^{-1} was also instigated by the Li^+ ions incorporation. The study demonstrated that MnS and lithium-doped MnS thin films are suitable electrode materials for energy harvesting and electrochemical energy storage devices.

Keywords: Photoabsorption, Energy storage, Cyclic voltammetry, Energy band gap, Pseudocapacitive, I-V characteristics

INTRODUCTION

Extensive research has been conducted on semiconductor sulfide materials due to their notable variations in synthesis methods, leading to diverse structures, sizes, and size distributions. As a result, these materials exhibit improved properties and offer promising prospects for various applications. These properties give nanocrystals diverse shapes, flexibilities and configurations to function as fundamental units for constructing and organizing nano devices. One-dimensional nanostructures, which have limited growth in two directions, demonstrate remarkable optical, mechanical, and electrical properties (Gajanan *et al*., 2011). Manganese chalcogenides (sulfides, selenides, and tellurides) have gained attention for their distinctive morphological, physical, and chemical characteristics. They belong to a class of semiconductors called diluted magnetic semiconductors (DMS) with band structures quite related to those of their host II-VI or III-V compounds, they exhibit the band structures of zinc-blende or wurtzite semiconductors, and, except for some III-V compounds, they have a direct band gap transition (Cibert and Scalbert, 2008). MnS thin films or powder can be found in several polymorphic forms: the green colored stable cubic modification having the rock-salt type structure (α-MnS) which is the most common, the metastable pink zinc-blende type (β-MnS), or the metastable wurtzite-type structure with (γ-MnS); at 100 - 400℃, it has been found that β and γ types can be transformed irreversibly to the stable α-type MnS. Generally, MnS are characterized by its wide band gap ($E_g \geq 3.02eV$). They are p-type semiconductors and hold promise for various applications such as solar cells, optical windows/buffer materials, optoelectronic devices, and luminescent materials (Gajanan, 2011; Honsberg, 2019). However, this characteristic combined with its poor electrical conductivity has limited its application. Factors such as the intricate mechanism of charge carrier production, lifespan, charge density, recombination,

defect sites, influence the material's conductivity. Many scientists have used band operational modulations from the introduction of sulphur vacancies to increase the conductivity of these materials because they are suitable for instigating holes to improve the passage of the charge carrier between the material's energy bands. To achieve this, many authors have adopted to incorporation of impurity such as dopant within the framework of the MnS host lattice. Among several dopants, mono-ionic dopant has offered several advantages over multi-charged dopant, one of which is the efficient introduction of charge carriers for improved conductivity with insignificant lattice distortion (Liu *et al*., 2022; Zhao *et al*., 2023). This minimizes unnecessary defect and consequently facilitates optimum stability and performance. Reviews have shown that there are many synthetic methods by which any of the three forms of MnS can be prepared. The methods encompass solvothermal method (Chang *et al*., 2021), hydrothermal method (Swathi *et al*., 2021), chemical bath deposition (Abbas *et al*., 2024), colloidal synthesis (Zhang *et al*., 2022), electrodeposition (Mandal *et al*., 2022), radio-frequency sputtering (Morita *et al*., 2022), and so on. In this study, we have employed electrodeposition technique to prepare for the first time, a novel Li-doped MnS nanostructure on conductive substrate. The electrodeposited technique adopted was a two-electrode mode involving the use of the substrate and carbon as working and counter electrodes, respectively. The authors also characterized the prepared films to investigate the effect of Li-ion impurity on optical, electrical and electrochemical properties MnS for potential in optoelectronics and energy storage applications.

MATERIALS AND METHODS

Materials

The study employed the use of electrolytic precursors prepared from high analytical grade (~97%, purity) inorganic chemical reagents: manganese sulphate monohydrate ($MnSO_4.H_2O$) and lithium chloride. Sodium thiosulphate pentahydrate ($Na_2S_2O_3.5H_2O$) solution was also prepared as sulphury source. Double distilled water (DW) was utilized as solvent for dissolution of the chemicals. Conductive ITO coated glass was purchased from Lumtec. Inc, China and employed as substrate as well as current collector for electrodeposition process and electrochemical charge storage testing. The ITO/glass substrates were first scrubbed with cotton bud in soapy water. Afterwards, they were ultrasonicated for 10 minutes (using acetone and distilled water). This process was necessary to maintain homogeneity and better quality of films. For the preparation of sample, two different solution electrolytes were prepared. Solution A was prepared from the reaction of 0.15 M of $MnSO_4.H_2O$ and 0.01 M of $Na_2S_2O_3.5H_2O$ in 100 mL DW, while solution B and C involve 0.02 mol % and 0.02 mol % LiCl of solution A in 100 mL DW, respectively. The solutions were prepared in separate beakers and stirred using magnetic stirrer until homogenous and clear solution was obtained.

Samples' preparation

Film growth was carried out by two-electrode mode encompassing the ITO/glass slide as the cathode and a carbon electrode (graphite) as the anode. The source of power supply for the process was a DC voltage source meter. Voltage drop and current degradation during the deposition were measured with the aid of a digital multimeter while the power supply was being kept under potentiostatic mode (1.8 V), throughout the experiments. Three separate film samples were prepared. Pristine MnS film sample was first produced from solution A precursor with the electrochemical deposition set up illustrated in our previous work [Taleatu *et al*., 2014]. The substrate was left in the solution until an optimum growth was observed via visual examination. The sample obtained was tagged sample 'M'. Following the same procedure, two different Li-doped MnS film samples (Li@MnS) were prepared from the mixture of solution B and C, with A based on the stated prescription. The samples were tagged sample LM1 and LM2, accordingly. After the synthesis process, all the samples were annealed at 300 ℃ for about 90 minutes in open air furnace to possibly remove adsorbed moisture and hence kept in air-tight container for characterization.

Samples' characterization

All the samples were measured to explore their optical, electrical and electrochemical charge storage characteristics. The optical measurements were carried out with the aid of absorbance and transmittance data collected for each sample using Shimadzu double beam spectrophotometer with the ultraviolet (UV)/visible light range of solar spectrum. The electrical properties of the samples were obtained using current-voltage (I-V) characteristic plots obtained using a four-point probe instrument. The electrochemical charge storage characteristics of the synthesized material were explored using their measured cyclic voltammetry (CV) curves under three-electrode configuration involving the deposited film sample, Ag/AgCl, and graphite as working, reference and counter electrode, respectively. The CV data were obtained from Corrtest potentiostat/electrochemical workstation. Extensive details about the facilities employed for these measurements have been given in our earlier reports [Adewinbi *et al*., 2020; Adewinbi *et al*., 2021].

RESULTS AND DISCUSSION

Optical absorption and transmittance and Optical energy band-gap value estimations,

Optical properties of thin film materials play a critical role in diverse applications such as optoelectronics, photovoltaics, and sensors. The spectral absorbance data of the deposited films was measured and their corresponding plots as a function of wavelength are presented in Figure 1(a). From the plots, it can be observed that that the absorbance of the films is generally high but decreases with an increase in wavelength. Furthermore, one could observe that the visible light absorption of the deposited MnS thin film increases at the Li-ion dopant content increases. These unique features are complemented with the one obtainable from their corresponding transmittance spectral depicted in Figure 1(b), as the enhanced incorporation of Li-ion dopant impurity reduced the visible light transmission properties of the deposited MnS thin film. The decrease in optical transmittance of MnS with increasing Li-dopant could be attributed to the enhanced grain boundaries during the introduction of dopant (Guo *et al*., 2020). The feature implies that the photabsorption of electrodeposited MnS host material can be improved via the incorporation of Li-dopant impurity. It also signifies that the higher the dopant content, the higher the light attenuation. It also suggests the material as an absorbent layer for solar cell applications and solar thermal energy collectors. (Onwuemeka and Ekpunobi, 2018). The energy bandgap is a vital factor influencing MnS thin films' optoelectronic characteristics and potential applications (Adewinbi *et al*., 2020). It represents the energy difference between the conduction band's lowest level and the valence band's highest level. Knowledge of bandgap gives understanding of light absorption and emission properties of MnS. With the aid of relation in Eq. (1) below, the absorption coefficient, (α) of the deposited film samples was calculated (Adewinbi *et al*., 2020).

$$\alpha = \frac{1}{d} \ln \frac{1}{T} \qquad (1)$$

where d and T represent the film thickness and transmittance data, respectively. The optical energy band gap value (Eg) for each film sample was estimated using Tauc's relation in the flowing Eq. (2) (Abbas et al., 2024).

$$(\alpha h\nu)^{1/\gamma} = B\,(h\nu - E_g) \qquad (2)$$

Where h is the Planck constant, ν is the photon's frequency, E_g is the band gap energy and B is a constant usually referred to as band parameters; the γ factor depends on the nature of the electron transition and is equal to ½ or 2 for direct and indirect transitions, respectively. The energy band gap value for each film sample is therefore estimated by extrapolating the linear portion of the corresponding plot of $(\alpha h\nu)^{1/\gamma}$ against $h\nu$ (photon energy) to a point where $\alpha h\nu = 0$ on the x-axis (Makula et al., 2018). The plots are shown in Figure 1(c), and the estimated Eg values for each sample are indicated on the corresponding plots as displayed. The decreasing band-gap value (2.03 to 1.85 eV) with Li-ion dopant incorporation, signifies a redshift feature characteristic which reaffirms enhanced photabsorption properties in the visible light spectra range of solar radiation, and indicates enhanced photocatalytic performance of MnS host material because of Li-dopant impurity incorporation. This feature also suggests the capability of the material for use as buffer layer for

recombination inhibition and enhanced charge transport properties of thin film organic solar cells. Furthermore, the estimated values of the band-gap are in good agreement with the previously reported data of CuMnS film by Ezenwaka et al. (2021). They conform to solar spectrum range, suggesting the films are good materials for photovoltaic cell application.

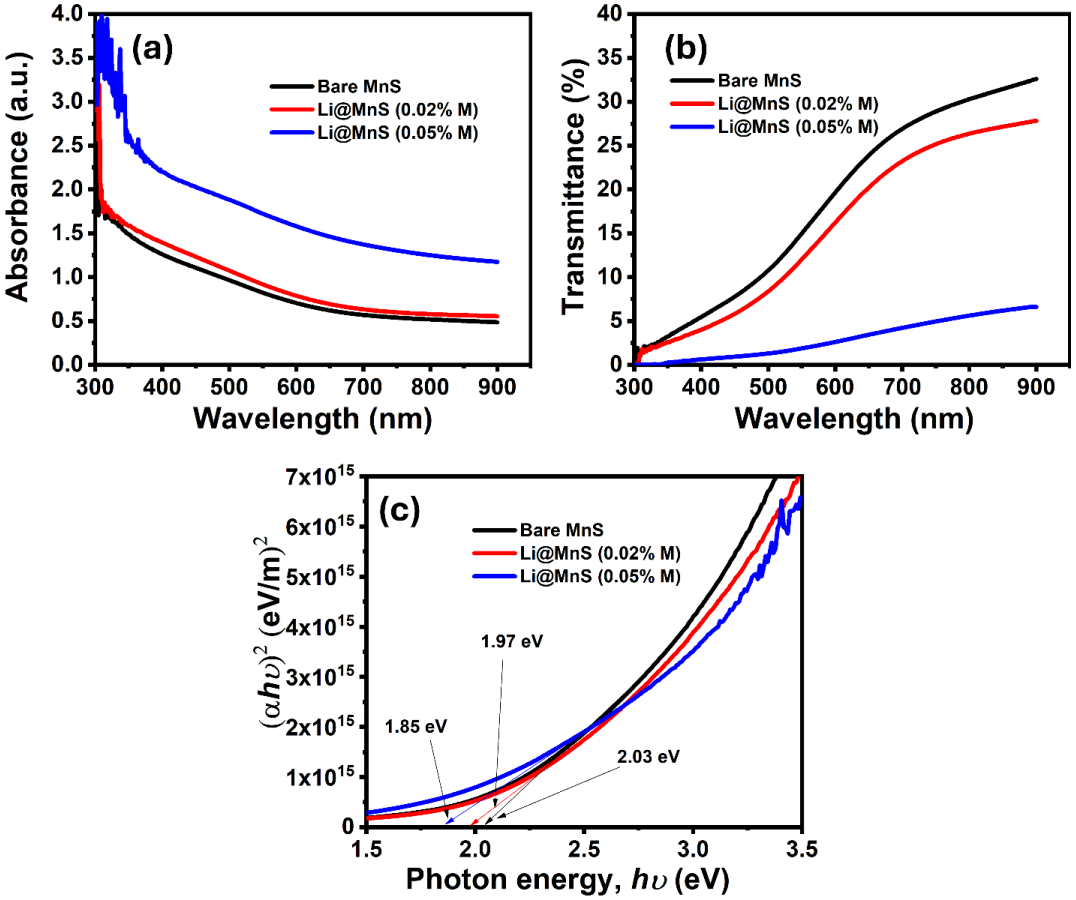

Figure 1: Optical measurements outputs (a) absorbance spectra (b) transmittance spectra and (c) Tauc plots for the estimation optical energy band gap of the deposited bare and Li-doped MnS thin films.

Film's extinction coefficient, refractive indices and optical conductivities

The extinction coefficients of film material determine how strongly a material absorbs or reflection light at particular wavelength. It is determined from absorption coefficient α using the relation given in Eq. (3) (Busari et al., 2020).

$$k = \frac{\lambda\alpha}{4\pi} \qquad (3)$$

The plots of extinction coefficients as function of photon energy for the samples are presented in Figure 2(a). Observable from the plots, the extinction coefficient of MnS, decays exponentially up to 1.78; and beyond 1.78 eV, it shows a gentle rise. It is also found reducing with Li-ions incorporation relative to film thickness. Thus, it can be concluded that the exponential decrease in extinction coefficient with an increase in photon energy represents that the fraction of light lost owing to scattering and enhanced absorbance. These observations could be supported by Beer-Lambert law of light absorption in transparent medium indicating that the proportion of absorbed light in a homogenous isotropic medium is independent of the intensity of the monochromatic incident light; and thus, successive layer absorbs an equal fraction of the incident light. According to Beer-Lambert law stated in Equation 4, the dependence of the sample thickness and absorption coefficient on photon energy of absorbed and transmitted light due to scattering can be determined using appropriate python code.

$$I = I_o\, e^{-\alpha t} \qquad (4)$$

Where Intensity of incident light is I_o and that of transmitted light is I. α and t are absorption coefficient and film thickness respectively. The loss factor decreases with increase in photon energy. Thus, refractive index of materials describes the amount of light that is reflected when reaching the interface. The refractive index n, was deduced using the relation in Equation 5 below:

$$n = \frac{1}{T_s} + \sqrt{\frac{1}{T_s - 1}} \qquad (5)$$

where T_s is the percentage transmission coefficient (Busari *et al.*, 2023). The corresponding plots for each sample are depicted in Figure 2(b). The refractive index of all the sample increased as the photon energy increased. Additionally, it can be observed that the refractive indices values for the deposited MnS film sample increased as the Li-dopant content is raised. These observable features play an important role in optical material search and in constructing anti-reflecting coatings for solar cells (Callister and Rethwisch, 2011). Optical conductivity (σ) of the deposited films was calculated using the relationship given in Eq. (6)

$$\sigma = \frac{\alpha \eta c}{4\pi} \qquad (6)$$

Where α is the absorption coefficient, η is the refractive index, and c is the speed of light. The plot of the optical conductivity of the deposited MnS and Li@MnS as a function of wavelength is displayed in Figure 2(c). It can be observed that all the samples have considerably high value of optical conductivity with the highest found in Li@MnS (0.05 M). These results show that the films display good optical conductivity (Yasmeen *et al.*, 2019). The increase in the optical conductivity observed with increasing dopant content can be attributed to the increase in the density of localized states in the energy band introduced by the dopant impurity (Ikhioya et al., 2022).

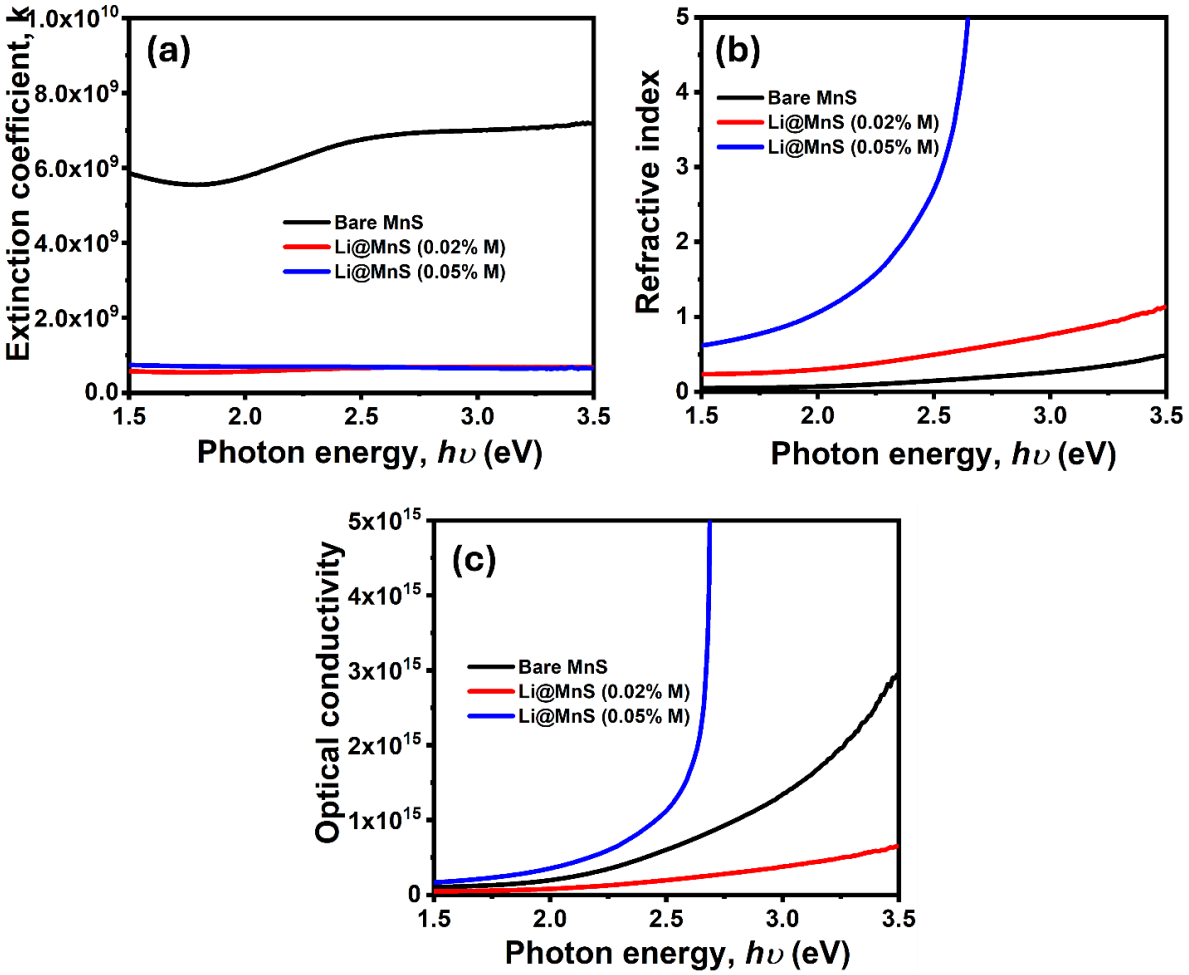

Figure 2: Plots of (a) extinction coefficient, (b) refractive indices, and (c) optical conductivity against photon energy for the deposited bare and Li-doped MnS thin films.

Electrical current-voltage (I-V) characteristics

The electrical properties of the films were investigated using a standard four-point probe technique. These were explored with the aid of each sample's corresponding I-V characteristic plot as depicted in Figure 3(a-b). It can be observed from the plots the measured current data showed a linear relationship with that applied voltage. These features signify the samples exhibited ohmic properties across the applied voltage range, indicating good electrical response (Adewinbi *et al.*, 2020). The results clearly show that the conductivity of the MnS host materials increased with the incorporation of Li dopant. The obtained resistivity and conductivity values as presented on each plot, accordingly, for each sample also demonstrate enhanced electrical response of the host materials upon dopant incorporation. It also corroborated the tailoring features of the optical energy bandgap with the dopant impurity.

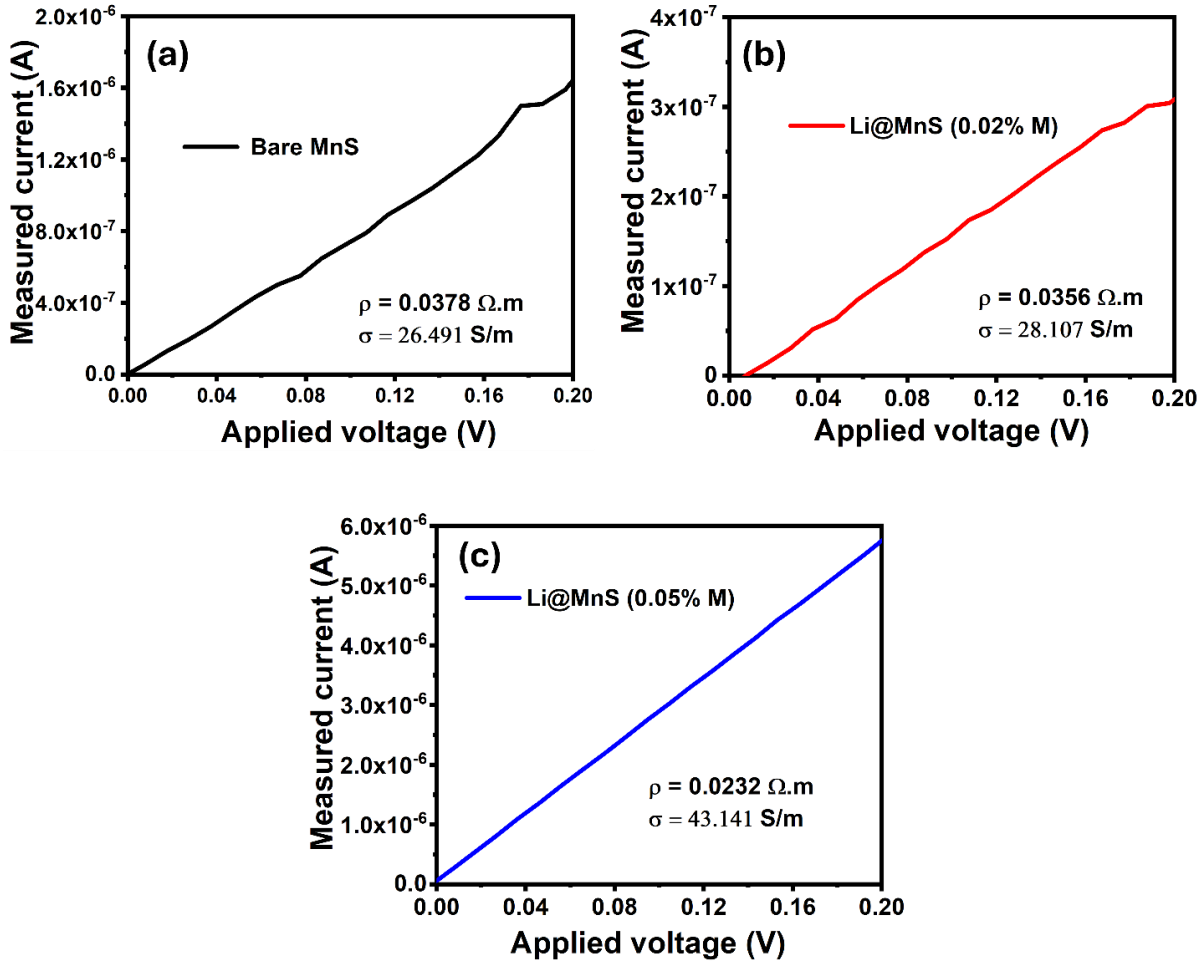

Figure 3: Current-voltage characteristic plots for the deposited (a) bare MnS, (b) Li@MnS (0.02% M) and (c) Li@MnS (0.05% M) thin films.

Electrochemical charge storage properties

The electrochemical energy storage performance of the demosited film samples as electrode prototype has been investigated using their respective CV curves as diplayed in Fig. 4(a-b). The measurement were taken at various scan rate (10 to 100 mV s^{-1}). Generally, it can be observed that the CV curves of all the sample dispalyed a quasi rectangular shapes with no significant redox peak. This feature signifies the exhibition of a typical pseudocapacitive behaviour by the electrode materials. The absence of redox peaks on the curves reavealed that charge-discharge volatmmetry behaviour of the electrodes is of high pseudoconstant rate (Adewinbi *et al.*, 2022). Additionally, there is no significant variation in the quasi rectangular shape of these curves with respect to the introduction of the dopant material. These featues can be ascribed to the inherent pseudocapacitive properties often associated with the Mn-based electrode material (Admuthe *et al.*, 2020; Adewinbi *et*

al., 2022). They are traceable to the faradiac reactions resulting from processes of intercalation/deintercalation of KOH electrolye ions within the electrode material. Area under the CV curves was found to increase with increasing dopant content, signifying enhanced current response MnS electrode with the incorporation of Li-dopant ion. This corroborates the observed I-V characteristic features revealing enhanced MnS electrode's electrical conductivity with increasing Li-ion dopant concentration. The linear increase in curve surface area under the CV plot with increasing scan rate feature of the all electrodes symbolizes enhanced rate capability. The specific capacitance (C_s) of electrode film sample was calculated with the aid of reation in Eq. (7) (Animasahun *et al.*, 2023).

$$C_s = \frac{1}{mS_rV}\int_{v_1}^{v_2} I(V)\,\mathrm{d}V \qquad (7)$$

Where, m, S_r, V, and $\int_{v_1}^{v_2} I(V)\,\mathrm{d}V$, represent mass of the active electrode films which were estimated from the weight differences of the blank and the coated ITO/glass substrate, scan rate, and integral areas of the CV curves. The specific capacitance values were estimated as 53.67, 94.46 and 73.38 F g^{-1} for the pristine MnS, Li@MnS (0.02M), and Li@MnS (0.05 M), respectively. The specific capacitance of the optimized sample was also measured with respect to varying scan rates. The plot is depicted in Fig. 4(c). Notably, the specific capacitance value reduced with an increasing scan rate. This observable feature is attributable to the fact that the electrolytic ions had enough time to access huge part of the electrode active film at lower scan rates (Adewinbi *et al.*, 2021). In summary, the MnS host film demonstrated enhanced supercapacitive charge storage performance with the incorporation of Li-ion dopant impurity within the host's framework.

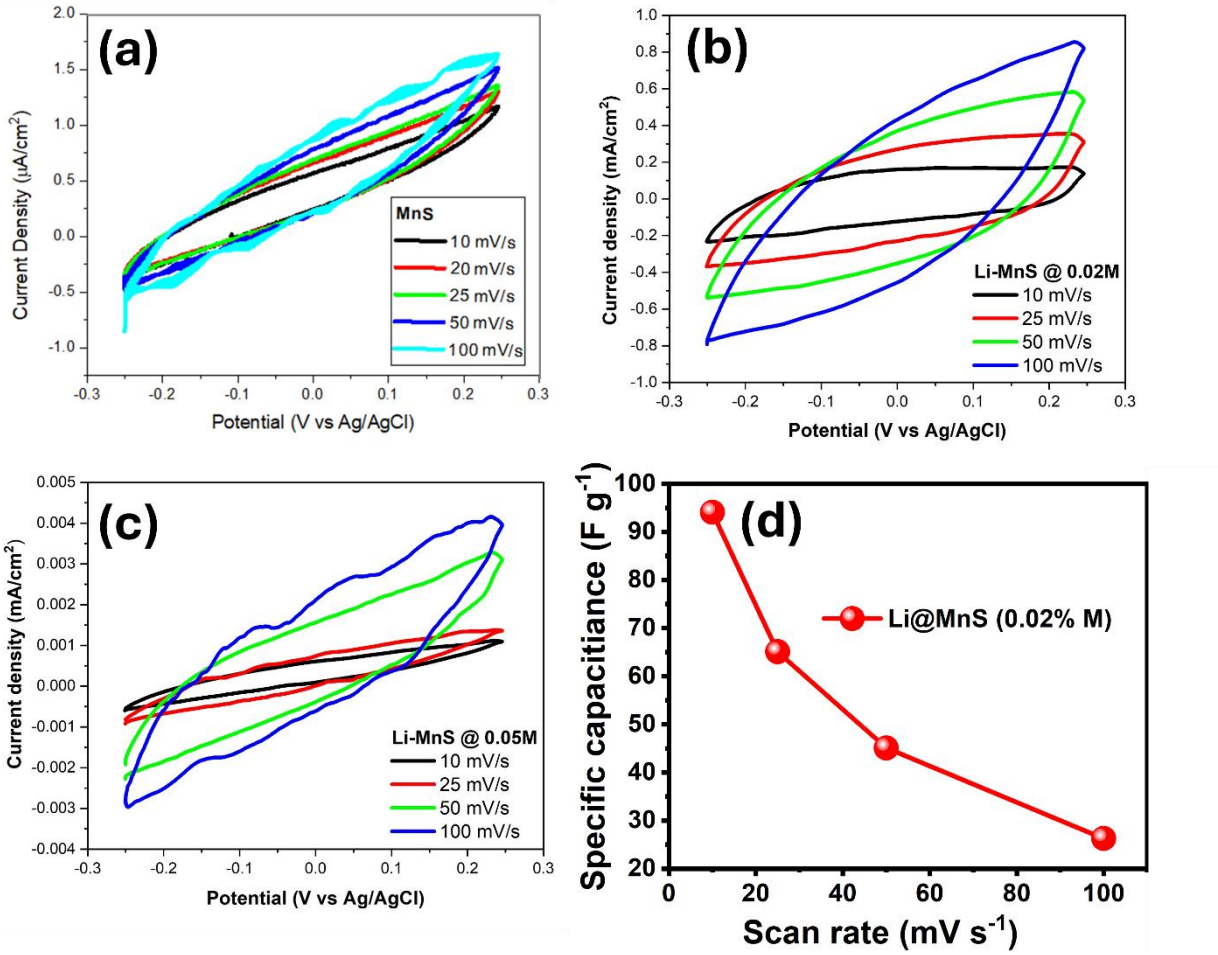

Figure 4: (a-c) Electrochemical C-V curves for the deposited bare MnS, Li@MnS (002% M) and Li@MnS (005% M) thin film electrodes at various scan rates, (d) plot of specific capacitance vs. scan rate for the optimum Li@MnS (0.02% M) thin electrode.

CONCLUSION

Lithium-doped manganese sulphide thin films with varying concentration (0.00, 0.02 and 0.05% molar) have been successfully prepared on ITO/glass substrate from suitable inorganic chemical reagents by electrochemical deposition technique because of its simplicity and low cost. It is also environment-friendly which does not require the use of hazardous solvent or reactive precursors. Optical, electrical and supercapacitor properties of the studied materials were investigated through UV-Vis spectroscopy, I-V and electrochemical cyclic voltammetry measurements, respectively. Measured optical parameters showed low transmittance and decreased band gap energies as the dopant concentration increased; the band gap energies of the thin films are 2.03 eV and 1.85 eV with increasing dopant concentration. Electrical studies revealed decreasing resistivity values and enhanced conductivity as the dopant concentration increased. In addition, the C-V curves showed that thin films exhibit pseudocapacitive behavior with enhanced specific capacitance value 95 F g^{-1} courtesy of high electrical conductivity induced by the Li-ion dopant incorporation. However, further investigations are required to establish the charge storage kinetics towards these capacitive outputs. These results show that these Li@MnS can be used as active photoabsorber layer in solar cell as well as active electrode material for electrochemical energy storage applications.

DECLARATION OF CONFLICT OF INTEREST

The authors declare no conflict of interest. They all participated in the formation of research problem, experimental work, results analyses and discussion as well as development of the manuscript.

REFERENCES

Abbas, H. W., Shafique, M., & Akhtar, M. S. (2024). Structural, Morphological and Optical Investigations of Pure and Iron Doped Manganese Sulfide Thin Film by Chemical Bath Deposition. *Journal of Nano Research, 86*, 51-56.

Adewinbi, S. A., B. A. Taleatu, R. A. Busari, O. E. Adewumi, E. Omotoso, K. O. Oyedotun, and N. Manyala. "Preparation and surface characterization of nanostructured MoO_3/Co_xO_y and V_2O_5/Co_xO_y interfacial layers as transparent oxide structures for photoabsorption." *Journal of Electronic Materials* 49 (2020): 3837-3848.

Adewinbi, S. A., Maphiri, V. M., Taleatu, B. A., Marnadu, R., Shkir, M., Hakami, J. & Gedi, S. (2022). Binder-less fabrication, some surface studies, and enhanced electrochemical performance of Co, Cu-embedded MnO_2 thin film electrodes for supercapacitor application. *Ceramics International*, *48*(18), 26312-26325.

Adewinbi, S. A., Taleatu, B. A., Busari, R. A., Maphiri, V. M., Oyedotun, K. O., & Manyala, N. (2021). Synthesis and electrochemical characterization of pseudocapacitive α-MoO_3 thin film as transparent electrode material in optoelectronic and energy storage devices. *Materials Chemistry and Physics*, *264*, 124468.

Admuthe, A., Kumbhar, S. S., Chougule, S. K., Padasare, G. N., & Tonape, M. M. (2020, August). Synthesis and characterization of MnS thin film at room temperature for supercapacitor application. In *Macromolecular Symposia* (Vol. 392, No. 1, p. 2000186).

Animasahun, L. O., Taleatu, B. A., Adewinbi, S. A., Busari, R. A., & Fasasi, A. Y. (2023). Binder-free fabricated transparent Nb4+ implanted Nb2O5-x ultra-thin negatrode with enhanced areal capacitance and exceptional cyclic stability in aqueous electrolyte. *Solid State Sciences*, *140*, 107204.

Busari, R. A., Taleatu, B. A., Adewinbi, S. A., Adewumi, O. E., Omotoso, E., Oyedotun, K. O., & Fasasi, A. Y. (2020). Synthesis and surface characterization of electrodeposited quaternary chalcogenide $Cu_2Zn_xSn_yS_{1+x+2y}$ thin film as transparent contact electrode. *Bulletin of Materials Science*, *43*, 1-9.

Busari, R.A., Omotoso, E., Animasahun, L.O., Adewinbi, S.A., Adewumi, E.O., Famoroti, C.T., Taleatu, B.A., & Fasasi, A.Y. (2023). Tuning the optical properties and some surface structure of Cd-O thin film electrodeposited by two-electrode: An effect of Cobalt incorporation. *Nigerian Society of Physical Sciences*, 5, 1222. 10.46481/jnsps.2023.1222.

Callister, W.D., & Rethwisch, D.G. (2011). *Materials Science and Engineering.* New York: Wiley
Chang, C. J., Teng, M. C., Chen, J., Lin, Y. G., & Chen, C. Y. (2021). Microwave solvothermal synthesis of cubic MnS@ Ag2S core-shell photocatalysts with improved charge separation and photocatalytic activity. *Applied Surface Science*, *558*, 149875.

Cibert, J. & Scalbert, D. (2008). Diluted Magnetic Semiconductors. In M. Dyakonov, *Spin Physics in Semiconductors* (pp. 389-431). Heidelberg, Berlin: Springer.

Ezenwaka, L.N., Nwori, A.N., Ottih, I.E., Okereke, N.A., & Okoli N.L. (2021). Investigation of the Optical, Structural and Compositional Properties of Electrodeposited Lead Manganese Sulfide (PbMnS) Thin Films for Possible Device Applications. *Universal Wiser Publisher*, 3(1), 18-32. https://doi.org/10.37256/nat.3120221226.

Gajanan, P., Harendra, K.S., Srivastava, S.K. & Kotnala, R.K. (2011). Gamma-MnS nano and micro architectures: Synthesis, characterization and optical properties. *Materials Research Bulletin*, 46(11), 1804-1810.

Guo, J., Lou, Q., Qiu, Y., Wang, Z. Y., Ge, Z. H., Feng, J., & He, J. (2020). Remarkably enhanced thermoelectric properties of Bi2S3 nanocomposites via modulation doping and grain boundary engineering. *Applied Surface Science*, *520*, 146341.

Honsberg, C.B., & Bowden, S.G. (2019). *MnS*. Retrieved from Photovoltaics Education: https://www.pveducation.org/pvcdrom/materials/mns

Ikhioya, I. L., Danladi, E., Nnanyere, O. D., & Salawu, A. O. (2022). Influence of precursor temperature on bi doped ZnSe material via electrochemical deposition technique for photovoltaic application. *Journal of the Nigerian Society of Physical Sciences*, 123-129.

Liu, Y., Zhou, X., Jia, Z., Wu, H., & Wu, G. (2022). Oxygen vacancy-induced dielectric polarization prevails in the electromagnetic wave-absorbing mechanism for Mn-based MOFs-derived composites. *Advanced Functional Materials*, *32*(34), 2204499.

Makula, P., Pacia, M., & Macyk, W. (2018). How to correct determine the band gap energy of modified semiconductor photocatalysts based on Uv-Vis spectra. *The Journal of Physical Chemistry Letters*, 9(23), 6814-6817.

Mandal, M., Chattopadhyay, K., Paria, S., Kundu, A., Chakraborty, M., Mal, S., ... & Bhattacharya, S. K. (2022). Electrodeposited binder-free Mn-Co-S nanosheets toward high specific-energy aqueous asymmetric supercapacitors. *ACS Applied Electronic Materials*, *4*(9), 4357-4367.

Morita, M., Ishibashi, K., Takahashi, K., Ueda, S., Chen, J., Tatejima, K., ... & Nagata, T. (2022). Effect of reactive gas condition on nonpolar AlN film growth on MnS/Si (100) by reactive DC sputtering. *Japanese Journal of Applied Physics*, *61*(SC), SC1071.

Onwuemeka, J.I., & Ekpunobi, A.J. (2018). Synthesis of CdO:SnO_2 alloyed thin films for solar energy conversion and optoelectronic applications. *Journal of Materials Science: Materials in Electronics*, 29, 9176-9183. https://doi.org/10.1007/s10854-018-8945-z.

Swathi, S., Yuvakkumar, R., Kumar, P. S., Ravi, G., & Velauthapillai, D. (2021). Hydrothermally synthesized α-MnS nanostructures for electrochemical water oxidation and photocatalytic hydrogen production. *Fuel*, *303*, 121293.

Taleatu, B. A., Arbab, E. A. A., Omotoso, E., & Mola, G. T. (2014). Synthesis and microstructural studies of annealed Cu_2O/Cu_xS bilayer as transparent electrode material for photovoltaic and energy storage devices. *Journal of Microscopy*, *256*(1), 61-71.

Yasmeen, S., Iqbal, F., Munawar, T., Nawaz, M.A., Asghar, M., & Hussain, A. (2019). Synthesis, structural and optical analysis of surfactant assisted ZnO–NiO nanocomposites prepared by homogeneous precipitation method. *Ceramics International*, 45(14), 17859-17873. https://doi.org/10.1016/j.ceramint.2019.06.001.

Zhang, Y., Cai, J., Wang, X., Lei, J., Wu, Q., Hu, Z., & Zhao, Z. (2022). Colloidal Synthesis of γ-MnS Nanorods with Uniform Controlled Size and Pure⟨ 002⟩ Growth Direction. *The Journal of Physical Chemistry Letters*, *13*(34), 8033-8037.

Zhao, C., Shu, J., Fang, J., Luo, S., Guo, Y., Xu, P., & Wang, L. (2023). Interface modification using Li-doped hollow titania nanospheres for high-performance planar perovskite solar cells. *ACS Applied Materials & Interfaces*, *15*(40), 46925-46932.